Article

Cell Reports

p27^{Kip1} Modulates Axonal Transport by Regulating α-Tubulin Acetyltransferase 1 Stability

Graphical Abstract

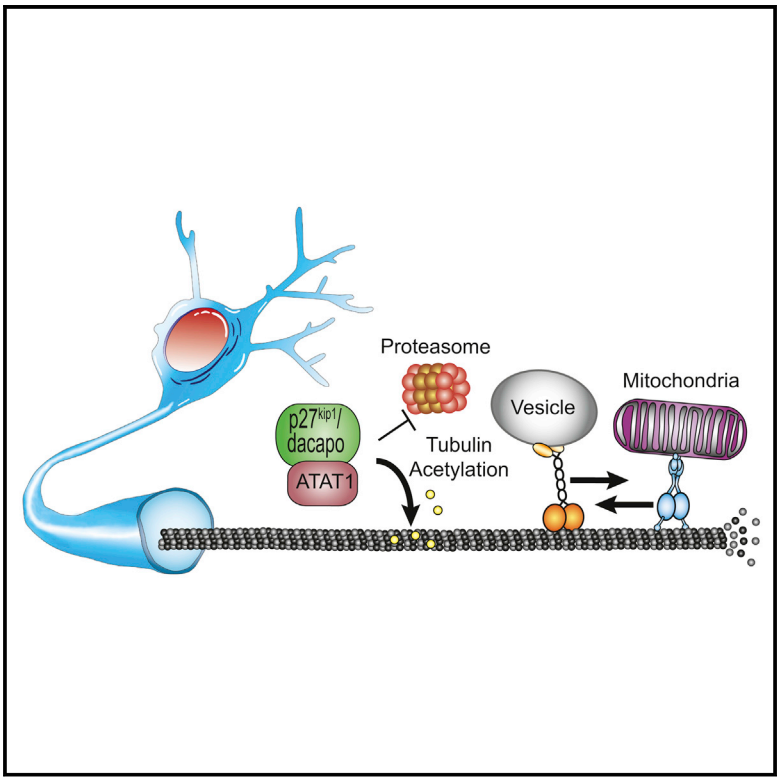

Authors

Giovanni Morelli, Aviel Even, Ivan Gladwyn-Ng, ..., Miguel Weil, Bert Brône, Laurent Nguyen

Correspondence

lnguyen@uliege.be

In Brief

Morelli et al. report that p27^{Kip1}/Dacapo modulates the acetylation of microtubules in axons via stabilization of ATAT1, the main α-tubulin acetyltransferase. Its conditional loss leads to the reduction of bidirectional axonal transport of vesicles and mitochondria *in vitro* in mice and *in vivo* in *Drosophila*.

Highlights

- Expression of p27^{Kip1}/Dacapo is required for proper molecular transport
- Loss of p27^{Kip1}/Dacapo impairs acetylation of microtubules
- p27^{Kip1} stabilizes ATAT1 via its C-terminal domain

Morelli et al., 2018, Cell Reports *23*, 2429–2442
May 22, 2018 © 2018 The Author(s).
https://doi.org/10.1016/j.celrep.2018.04.083

CellPress

Cell Reports
Article

OPEN ACCESS
CellPress

p27^{Kip1} Modulates Axonal Transport by Regulating α-Tubulin Acetyltransferase 1 Stability

Giovanni Morelli,[1,2,8] Aviel Even,[3,8] Ivan Gladwyn-Ng,[1] Romain Le Bail,[1] Michal Shilian,[3] Juliette D. Godin,[7] Elise Peyre,[1] Bassem A. Hassan,[4] Arnaud Besson,[5,6] Jean-Michel Rigo,[2] Miguel Weil,[3] Bert Brône,[2] and Laurent Nguyen[1,9,*]

[1]Liege Université, GIGA-Neurosciences, Interdisciplinary Cluster for Applied Genoproteomics (GIGA-R), 4000 Liège, Belgium
[2]Universiteit Hasselt, BIOMED, 3500 Hasselt, Belgium
[3]Laboratory for Neurodegenerative Diseases and Personalized Medicine, Department of Cell Research and Immunology, The George S. Wise Faculty for Life Sciences, Sagol School of Neurosciences, Tel Aviv University, Ramat Aviv, 69978 Tel Aviv, Israel
[4]Sorbonne Universités, UPMC Université Paris 06, Inserm, CNRS, AP-HP, Institut du Cerveau et la Moelle (ICM)-Hôpital Pitié-Salpêtrière, Boulevard de l'Hôpital, 75013 Paris, France
[5]Institut National de la Santé et de la Recherche Médicale Unité Mixte de Recherche 1037, Cancer Research Center of Toulouse, 31037 Toulouse, France
[6]Centre National de la Recherche Scientifique, ERL 5294, Université de Toulouse, Université Paul Sabatier, 31037 Toulouse, France
[7]Institut de Génétique et de Biologie Moléculaire et Cellulaire, 67404 Illkirch, France, CNRS U7104/INSERM U964, Illkirch, France
[8]These authors contributed equally
[9]Lead Contact
*Correspondence: lnguyen@uliege.be
https://doi.org/10.1016/j.celrep.2018.04.083

SUMMARY

The protein p27^{Kip1} plays roles that extend beyond cell-cycle regulation during cerebral cortex development, such as the regulation of neuronal migration and neurite branching via signaling pathways that converge on the actin and microtubule cytoskeletons. Microtubule-dependent transport is essential for the maturation of neurons and the establishment of neuronal connectivity though synapse formation and maintenance. Here, we show that p27^{Kip1} controls the transport of vesicles and organelles along the axon of mice cortical projection neurons *in vitro*. Moreover, suppression of the *p27^{Kip1}* ortholog, *dacapo*, in *Drosophila melanogaster* disrupts axonal transport *in vivo*, leading to the reduction of locomotor activity in third instar larvae and adult flies. At the molecular level, p27^{Kip1} stabilizes the α-tubulin acetyltransferase 1, thereby promoting the acetylation of microtubules, a post-translational modification required for proper axonal transport.

INTRODUCTION

Axonal transport of vesicles and organelles is essential for the functional differentiation of neurons as well as for establishment of their connectivity (Maday et al., 2014). Anterograde and retrograde transport of cargoes and organelles are mediated by microtubule (MT)-anchored molecular motors of the kinesin and dynein superfamilies, respectively. Axonal transport is a dynamic process that is critical for regulating the homeostasis of neuronal synapses (Maday et al., 2014). Anterograde transport replenishes the presynaptic sites and the axons with protein supply, and retrograde transport allows the recycling or removal of proteins and organelles from the axon terminals (Maday et al., 2014). Hence, disruption in axonal transport can result in aberrant synaptic functions, leading to neurodevelopmental and neurodegenerative disorders (Millecamps and Julien, 2013; Poirier et al., 2013).

Several proteins that either bind or modify the MTs are important for the regulation of axonal transport (Baird and Bennett, 2013). Within this context, impaired acetylation of α-tubulin results in the decreased binding of molecular motors to MTs, thereby leading to a reduction in the velocity of organelles and vesicles (Dompierre et al., 2007; Godena et al., 2014; Reed et al., 2006). This post-translational modification is regulated by the antagonistic activities of the α-tubulin acetyltransferase 1 (ATAT1) and the MT-associated deacetylase HDAC6 (Friedmann et al., 2012; Hubbert et al., 2002). It is interesting that depletion of the Cip/Kip family member p27^{Kip1} has been associated with poorly acetylated α-tubulin in MTs (Baldassarre et al., 2005). Indeed, in addition to promoting cell-cycle exit (Fero et al., 1996), p27^{Kip1} has multifunctional roles that extend beyond cell-cycle regulation during the establishment of the cerebral cortex, which require cytoplasmic activity on the cytoskeleton either via its components or regulators (Godin et al., 2012; Kawauchi et al., 2006; Nguyen et al., 2006a).

Here, we show that the neuronal depletion of p27^{Kip1} in mice or its ortholog, *dacapo*, in *Drosophila melanogaster* disrupts the axonal transport of organelles *in vitro* and *in vivo*, respectively. At the molecular level, p27^{Kip1} decorates axons and is required for proper acetylation of MTs via stabilization of ATAT1. Taken together, our data show that p27^{Kip1} modulates axonal transport regulation by promoting α-tubulin acetylation.

RESULTS

Non-canonical Activity of p27^{Kip1} in Axonal Transport of Cortical Projection Neurons

Because p27^{Kip1} is expressed by post-mitotic cortical neurons (Nguyen et al., 2006a; Kawauchi et al., 2006) and is associated with MTs (Godin et al., 2012), we postulated the existence of a

This is an open access article under the CC BY-NC-ND license (http://creativecommons.org/licenses/by-nc-nd/4.0/).

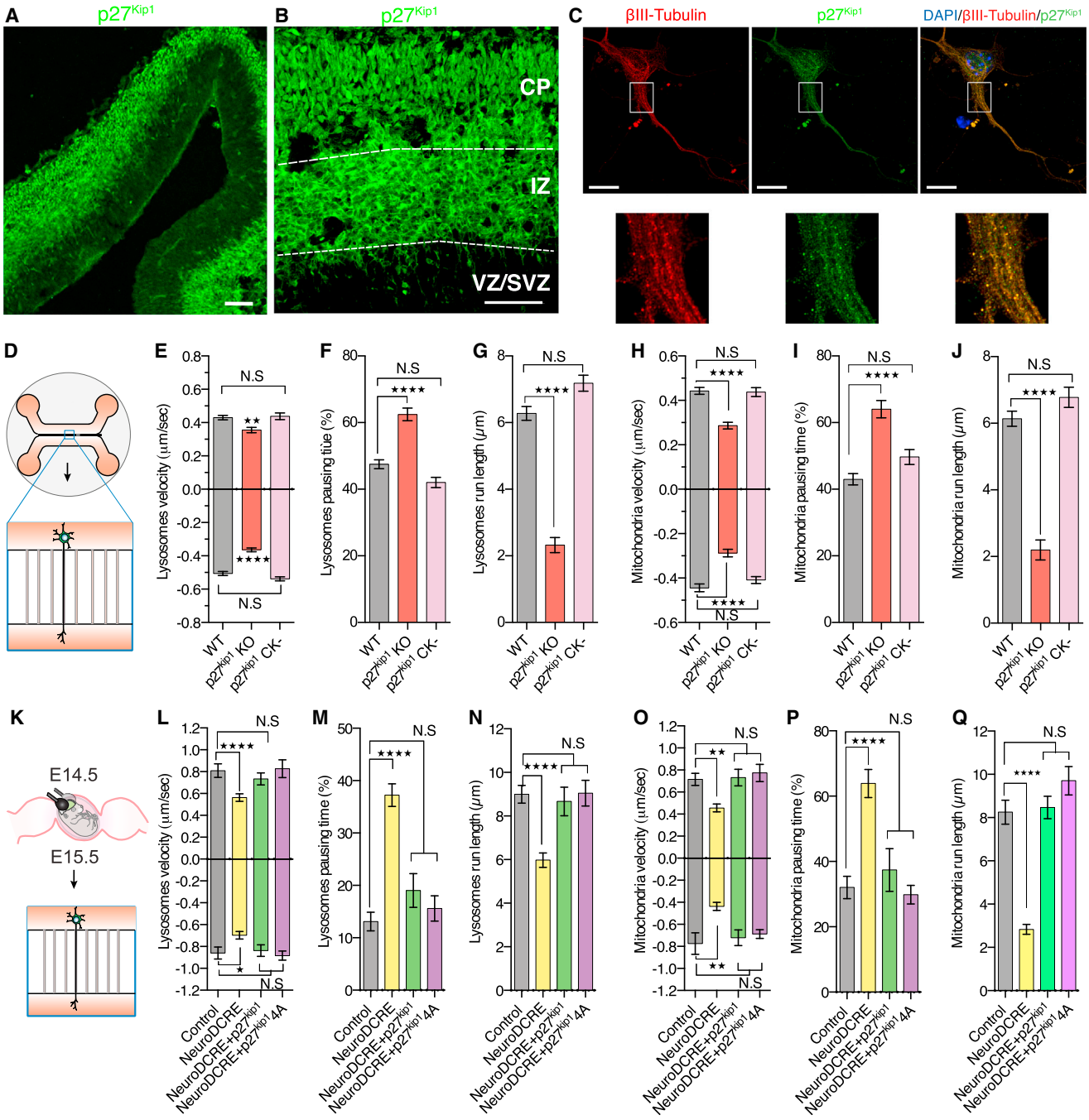

Figure 1. Depletion of p27^{Kip1} Disrupts Axonal Transport Independent of Its Cell-Cycle and MT-Polymerization Activity

(A and B) Representative immunolabelings showing p27^{Kip1} (green) expression pattern in the dorsal telencephalon of E14.5 mouse (A) or magnified field of the cortical wall (B). Scale bars, 100 μm.

(C) Super-resolution images and their magnifications of p27^{Kip1} (green), βIII-tubulin (red), and DAPI (blue) of cortical projection neurons cultured 7 DIV. Scale bar, 10 μm.

(D–J) Experimental setup for time-lapse recording of molecular transport parameters in axons from WT or *p27^{Kip1}* KO E14.5 mouse projection neurons cultured 7 DIV in microfluidic devices (D) to analyze instantaneous velocity (E and H), pausing time (F and I), and run length (G and J) of lysosomes (LysoTracker) and mitochondria (MitoTracker), as indicated on the histograms.

(E–J) Kruskal-Wallis ANOVA followed by Dunn post hoc comparison test. Number of vesicles and mitochondria >500, harvested from six (WT), five (*p27^{Kip1}* KO), and four (*p27^{Kip1}* CK-) embryonic mice. For instantaneous velocity of cargoes (E and H), $p = 0.0066$ for anterograde and $p < 0.0001$ for retrograde lysosomes; $p < 0.0001$ for anterograde and $p < 0.0001$ for retrograde mitochondria. For pausing time (F and I), $p < 0.0001$ for both lysosomes and mitochondria. For run length (G and J), $p < 0.0001$ for both lysosomes and mitochondria.

(legend continued on next page)

functional role for this protein in axonal transport. Immunolabeling of forebrain sections from embryonic day (E) 14.5 mice showed an accumulation of $p27^{Kip1}$ in the intermediate zone (IZ) and the cortical plate (CP), as compared to the proliferative ventricular zone (VZ) and subventricular zone (SVZ; Figures 1A and 1B). We assessed the subcellular distribution of $p27^{Kip1}$ in cortical neurons dissociated from E14.5 mouse embryos and cultured for 7 days *in vitro* (DIV). Immunolabeling revealed a predominant cytoplasmic distribution of $p27^{Kip1}$ in these neurons (Figure 1C), the specificity of which was confirmed further by immunolabeling and western blotting (WB) assays (Figures S1A and S1B). Our data show that $p27^{Kip1}$ is present in multiple subcellular compartments, including dendrites and axons. These findings are consistent with previous reports describing cell-cycle-independent activities for $p27^{Kip1}$ in the developing cerebral cortex (Kawauchi et al., 2006; Nguyen et al., 2006a).

Next, we assessed whether $p27^{Kip1}$ plays a role in axonal transport in isolated cortical projection neurons from E14.5 embryos that were cultured 7 DIV in microfluidics devices (Figure 1D). We recorded the axonal transport of lysosomes and mitochondria by time-lapse confocal microscopy using fluorescent probes (MitoTracker and LysoTracker, respectively). We found that projection neurons from $p27^{Kip1}$ knockout (KO) embryos displayed reduced instantaneous and average transport velocities of lysosomes and mitochondria, as compared to wild-type (WT) controls. These defects were associated with prolonged pausing time and diminished run length of vesicles and mitochondria (Figures 1D–1J and S2A–D) without affecting their moving directionality (Figures S2A, S2B, S2E, and S2F). Such defects were not observed in projection neurons isolated from $p27^{Kip1}$CK- mice (knockin mice expressing a cell-cycle dead variant of $p27^{Kip1}$ that cannot bind to cyclins and cyclin-dependent kinases [CDKs] [Besson et al., 2004]) (Figures 1D–1J and S2A–S2F), which indicate that $p27^{Kip1}$ modulates axonal transport via a cell-cycle-independent activity.

The projection neurons from E14.5 $p27^{Kip1}$ KO embryos preserved MTs architecture without major disruption of the axonal tracks (Figure S2G). However, previous work from our laboratory identified $p27^{Kip1}$ as a microtubule-associated protein (MAP) that promotes MT polymerization in migrating cortical interneurons (Godin et al., 2012). This activity is shared with other MAPs and is important in shaping MT tracks for motor protein-dependent transport. Therefore, we tested whether the axonal transport defects in neurons lacking $p27^{Kip1}$ may result from poorly polymerized MTs. To this end, we conditionally deleted $p27^{Kip1}$ in post-mitotic cortical projection neurons by *in utero* electroporation of NeuroD-Cre:GFP plasmids in E14.5 $p27^{Kip1}$ lox/lox embryos. The following day, neuron progenitors from electroporated embryonic brains were isolated and cultured 7 DIV in microfluidic devices to analyze the axonal transport of lysosomes and mitochondria (Figure 1K). Similar to $p27^{Kip1}$ KO mice projection neurons (Figures 1D–1J and S2A–S2F), the instantaneous and average transport velocities of lysosomes and mitochondria were reduced (Figures 1K, 1L, and 1O and S2H–S2K), while the moving directionality of lysosomes and mitochondria remained unchanged (Figures S2H, S2I, S2L, and S2M). These defects were associated with increased pausing time and shortened run length in $p27^{Kip1}$ lox/lox neurons electroporated with NeuroD-Cre:GFP, as compared to controls (Figures 1M, 1N, 1P, and 1Q and S2H–S2M). Re-expression of WT $p27^{Kip1}$ or its MT's polymerization dead variant, $p27^{Kip1}$ 4A (Godin et al., 2012), fully rescued bidirectional axonal transport defects of both lysosomes and mitochondria, without detectable differences between the $p27^{Kip1}$ full-length WT or $p27^{Kip1}$ 4A (Figures 1K–1Q and S2H–S2M). In summary, these results support the post-mitotic role of $p27^{Kip1}$ in axonal transport, which is independent of its MTs' polymerization activity.

The *Drosophila* $p27^{Kip1}$ Ortholog Dacapo Underlies Axonal Transport and Motor Behavior

Both murine $p27^{Kip1}$ and fly Dacapo promote cell-cycle exit (Fero et al., 1996; de Nooij et al., 1996), share amino acid sequence homologies (Figure S3A), and bind to and promote the polymerization of MTs (Figures S3B–S3E). Consistent with our observations in mouse neurons (Figures 1A–1C), Dacapo was immunodetected in the third larvae instar brain and axons of motoneurons (Figure 2A). We further crossed the upstream activating sequence (UAS):*dacapo*-RNAi fly line, with flies encoding the motoneurons' specific driver D42:Gal4 (*dap* KD), showing reduced expression of Dacapo in motoneurons (Figures S3F and S3G). Next, we confirmed the efficiency of the RNAi knockdown by crossing UAS:*dacapo*-RNAi flies with others expressing the Gal4 driver under a ubiquitous promoter (actin:Gal4 flies) (Figures S3H and S3I).

While the integrity of MTs was not affected in *dap* KD (Figure S4A), their third instar larvae displayed tail-flipping phenotype (Figure 2B) (30% of larvae) as compared to controls (*zpg* RNAi, "Control"), which suggests impaired axonal transport in motoneurons (Horiuchi et al., 2005). Further indications for impaired axonal transport in these neurons were supported by the analysis of locomotor behaviors. This analysis showed reduced crawling speed and peristaltic waves in *dap* KD third instar larvae (Figures 2C and 2D), as well as climbing defects in *dap* KD adult flies (Figure 2E) that were genetically rescued by conditional re-expression of *dap* ("Rescue") (Figures 2C–2E). The number and morphology of presynaptic boutons labeled

(K–Q) Experimental setup for time-lapse recording of molecular transport parameters in axons from $p27^{Kip1}$ lox/lox E14.5 mice embryos, *in utero* electroporated with either NeuroD-GFP (Control), NeuroD-Cre:GFP, NeuroD-CRE:GFP+$p27^{Kip1}$ or NeuroD-Cre:GFP+$p27^{Kip1}$ 4A, and cultured at E15.5 for 7 DIV in microfluidics devices (K) to analyze transport parameters, including instantaneous velocity (L and O), pausing time (M and P), and run length (N and Q) of lysosomes (LysoTracker) or mitochondria (MitoTracker). See also Figures S1 and S2.

(L–Q) Kruskal-Wallis ANOVA followed by Dunn post hoc comparison test. Number of vesicles and mitochondria analyzed per condition >500, harvested from three (NeuroD-GFP), three (NeuroD-Cre:GFP), four (NeuroD-Cr:GFP+$p27^{Kip1}$), and four (NeuroD-Cre:GFP+$p27^{Kip1}$ 4A) embryonic mice. For instantaneous velocity of cargoes (L and O), $p < 0.0001$ for anterograde and $p = 0.0183$ for retrograde lysosomes; $p = 0.0031$ for anterograde and $p = 0.00019$ for retrograde mitochondria. For pausing time (M and P), $p < 0.0001$ for both lysosomes and mitochondria. For run length (N and Q), $p < 0.0001$ for both lysosomes and mitochondria.

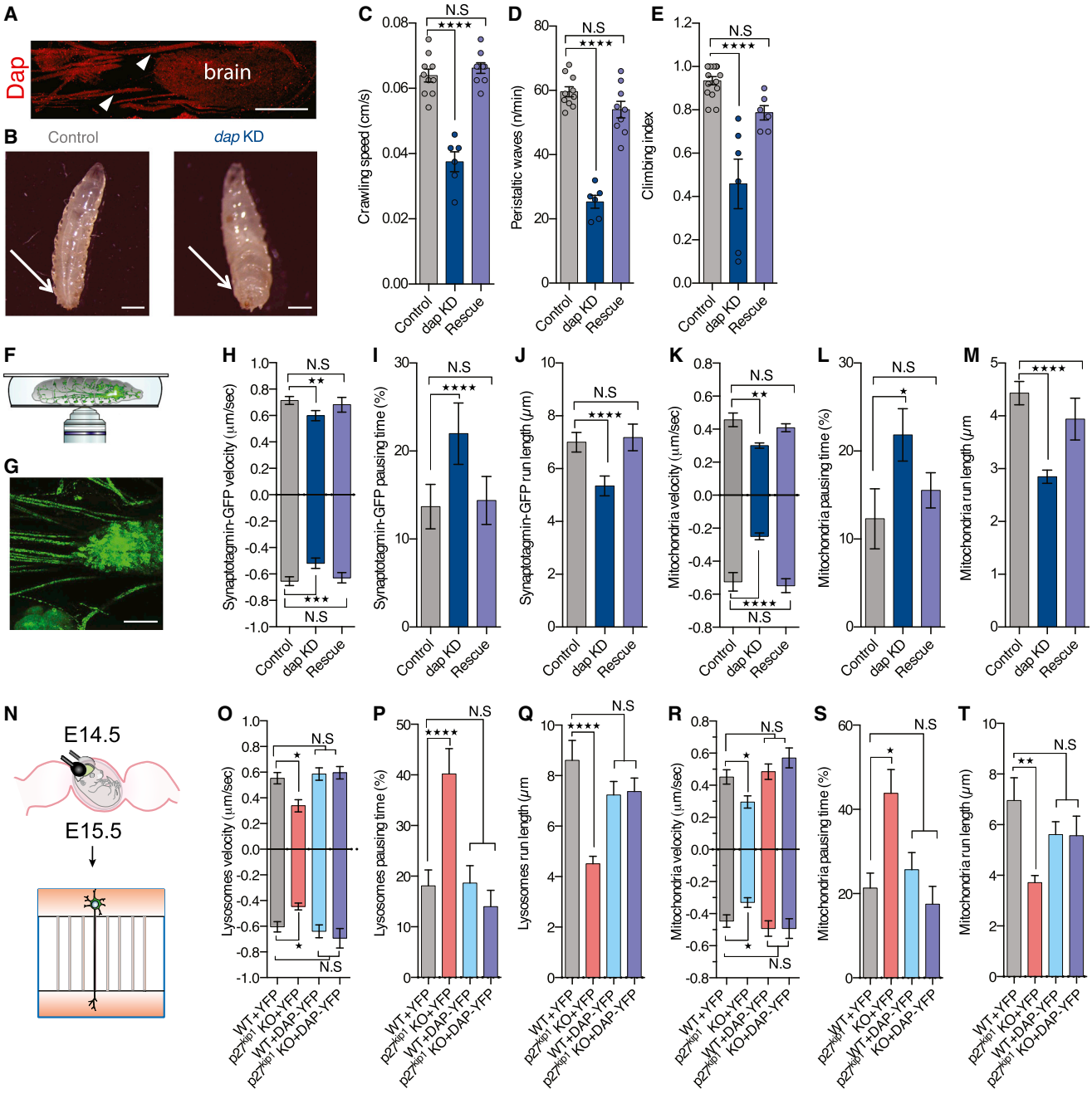

Figure 2. Depletion of Dacapo Disrupts Axonal Transport *In Vivo*

(A) Representative immunolabeling image of Dacapo (red) in a third instar larvae brain. Arrows indicate motoneurons departing from the brain. Scale bar, 60 μm.

(B) Representative image of tail-flipping phenotype in dap KD third instar larvae compared to Control larvae. Scale bars, 0.5 mm.

(C and D) Histograms of crawling speed (C) and peristaltic waves (D) of Control, dap KD, and Rescue third instar larvae. One-way ANOVA followed by the Bonferroni post hoc test. N for animals = 10 (Control), 6 (dap KD), and 9 (Rescue) ($p < 0.0001$; $F = 34.99$ for peristaltic waves; $p < 0.0001$; $F = 44.20$ for crawling speed).

(E) Histogram of climbing index for Control, dap KD, and Rescue adult flies. Kruskal-Wallis ANOVA followed by Dunn post hoc tests. N for groups of 10 adults = 13 (Control), 6 (dap KD), and 6 (Rescue) ($p < 0.0001$).

(F–M) Experimental setup for of *in vivo* live imaging of third instar larvae motoneuron axons (expressing Mito-GFP in green; scale bar, 60 μm) to analyze transport parameters (F and G), including instantaneous velocity (H and K), pausing time (I and L), and run length (J and M) of synaptotagmin-GFP or Mito-GFP.

(N–T) Experimental setup for time-lapse recording of molecular transport parameters in axons from projection neurons of $p27^{Kip1}$ KO E14.5 mice embryos, *in utero* electroporated with either Dacapo (DAP-YFP) or Control (YFP) plasmids, and cultured at E15.5 for 7 DIV in microfluidics devices to analyze transport

(legend continued on next page)

by cysteine string protein (CSP) in the neuromuscular junctions of third instar larvae were comparable between genotypes, suggesting that these behavioral defects did not arise from major synaptic alterations (Figures S4B and S4C).

Therefore, we used the third instar larvae of *dap* KD or Control (Figures S3F and S3G) to further probe the association between the behavioral phenotypes and axonal transport defects in motoneurons *in vivo*. We performed time-lapse confocal microscopy on third instar larvae motoneurons to record the movement of vesicles and mitochondria using genetically encoded synaptotagmin-GFP (synaptic vesicles), LAMP1-GFP (lysosomes), and Mito-GFP (mitochondria) (Zala et al., 2013). Recording of *dap* KD larvae showed a reduction in instantaneous and average transport velocities, which were associated with prolonged pausing times and reduced run lengths for both vesicles and mitochondria (Figures 2F–2M and S4D–S4L). These defects were comparable to the ones that were observed in the cortical projection neurons depleted for *p27^{Kip1}* (Figures 1D–1J andS2A–S2D). To confirm that Dacapo and p27^{Kip1} share similar activity in axonal transport, we replaced p27^{Kip1} by Dacapo in cortical projection neurons via *in utero* electroporation of Dacapo (DAP-YFP) into E14.5 or WT embryos (Figure 2N). The following day, electroporated neuronal progenitors were isolated and cultured for 7 DIV in microfluidic devices to track axonal transport of lysosomes and mitochondria (Figure 2N). Expression of Dacapo-YFP but not YFP (Control) rescued all axonal transport defects occurring upon the loss of p27^{Kip1} (instantaneous and average transport velocities, pausing time, and run length) (Figures 2O–2T and S4M–S4P) without affecting the directionality of moving vesicles and mitochondria (Figures S4M, S4N, S4Q, and S4R). These data demonstrate that p27^{Kip1} and its ortholog Dacapo share a common role in axonal transport in vertebrates (*Mus musculus*) and invertebrates (*D. melanogaster*), respectively.

Loss of p27^{Kip1} or Dacapo Results in Axonal Transport Defects that Can Be Rescued by Increasing Acetylation of MTs

Molecular transport is modulated by MAPs but also post-translational modifications occurring on MTs (Janke and Bulinski, 2011). Among these modifications, acetylation of α-tubulin K40 residues increases the recruitment of molecular motors on MTs and thus modulates axonal transport (Dompierre et al., 2007; Godena et al., 2014; Reed et al., 2006). WB analyses of cortical extracts isolated from P0 *p27^{Kip1}* KO mice showed a reduced level of acetylated α-tubulin, as compared to Controls (Figures S5A and S5B), which was reported previously in fibroblasts (Baldassarre et al., 2005). These data were further supported by immunolabeling of cultured projection neurons isolated from E14.5 WT or *p27^{Kip1}* KO mouse embryos (Figures S5C and S5D). Treatment with the selective HDAC6 inhibitor tubastatin (TBA, 10 μM) (Butler et al., 2010) rescued MT-acetylation-level in cultured *p27^{Kip1}* KO neurons (Figures 3A and 3B). In congruence, *dap* KD larvae showed reduced acetylation of α-tubulin in motoneurons, as compared to Controls, which was rescued either by genetic re-expression of *dap* (Rescue) (Figures S5E and S5F), or by feeding larvae with TBA-containing food for 30 min before recording (Figures 3C and 3D).

We further tested whether axonal transport defects observed *in vitro* in *p27^{Kip1}* KO cortical neurons and in *dap* KD motoneurons *in vivo* resulted from reduced acetylation of α-tubulin in MTs. We performed time-lapse recordings to assess the axonal transport of vesicles or mitochondria in mouse cortical neurons or in third instar larvae motoneurons preincubated with TBA for 8 hr and 30 min, respectively (Butler et al., 2010; Godena et al., 2014). TBA rescued axonal transport velocities of cargoes in both mouse cortical neurons and motoneurons from *Drosophila* larvae without affecting the directionality of moving vesicles and mitochondria (examined in mice) (Figures 3E–3P and S6A–S6O). More important, *dap* KD larvae incubated with sucrose solution supplemented with TBA also showed improved locomotor behavior (crawling speed and peristaltic movements of larvae) (Figures S6P and S6Q). Comparable ameliorations were observed after feeding flies with TBA-supplemented food for 5 days (climbing index) (Figure S6R). Taken together, these data suggest that reduction of the acetylation of MTs underlies the axonal transport defects observed in neurons from *p27^{Kip1}* KO mice or *dap* KD larvae, which further interfere with some motor behavior.

p27^{Kip1} Modulates the Acetylation of MTs by Stabilizing ATAT1

Members of the Cip/Kip family have no reported enzymatic activity and are thus unlikely to directly promote post-translational modifications of MTs. Because p27^{Kip1} can modulate gene transcription (Gallastegui et al., 2017), we analyzed P0 cortical extracts to assess the expression level of *aTAT1* and *Hdac6* mRNAs, which code for the main enzymes that regulate α-tubulin acetylation. Although no differences at the transcriptional level were observed between WT and *p27^{Kip1}* KO mice (Figures 4A and 4B), the protein level of ATAT1 but not HDAC6 was reduced upon loss of *p27^{Kip1}* (Figures 4C–4E). These data were supported further by immunolabeling cortical neurons electroporated *in utero* at E14.5 with ATAT1-GFP. The expression level of ATAT1-GFP was slightly reduced in p27^{Kip1} KO projection neurons, as compared to Control (Figures S7A and S7B). Conversely, overexpression of p27^{Kip1}:red fluorescent protein (RFP) in HEK293 cells resulted in the accumulation of ATAT1-GFP protein

parameters (N): instantaneous velocities (O and R), pausing time (P and S), and run length (Q and T) of lysosomes (LysoTracker) or mitochondria (Mitotracker). See also Figures S3 and S4.

(H–M and O–T) Kruskal-Wallis ANOVA followed by Dunn post hoc comparison test. (H–M) N for vesicles or mitochondria >200; N for animals = 20 (Control), 22 (dap KD), and 15 (Rescue). For instantaneous velocity of cargoes. (H and K), $p = 0.0025$ for anterograde and $p = 0.0003$ for retrograde vesicles; $p = 0.0056$ for anterograde and $p < 0.0001$ for retrograde mitochondria. For pausing time (I and L), $p < 0.0001$ for vesicles and $p = 0.0247$ for mitochondria. For run length (J and M), $p < 0.0001$ for vesicles and mitochondria. (O–T) N for lysosomes or mitochondria >150; N for animals = 3 (WT+YFP), 3 (WT+DAP-YFP), 3 (p27^{Kip1} KO+YFP), and 3 (p27^{Kip1} KO+DAP-YFP). For instantaneous velocity of cargoes (O and R), $p = 0.0318$ for anterograde and $p = 0.0191$ for retrograde lysosomes; $p = 0.0447$ for anterograde and $p = 0.0493$ for retrograde mitochondria. For pausing time (P and S), $p < 0.0001$ for lysosomes and $p = 0.0164$ for mitochondria. For run length (Q and T), $p < 0.0001$ for lysosomes and $p = 0.0039$ for mitochondria.

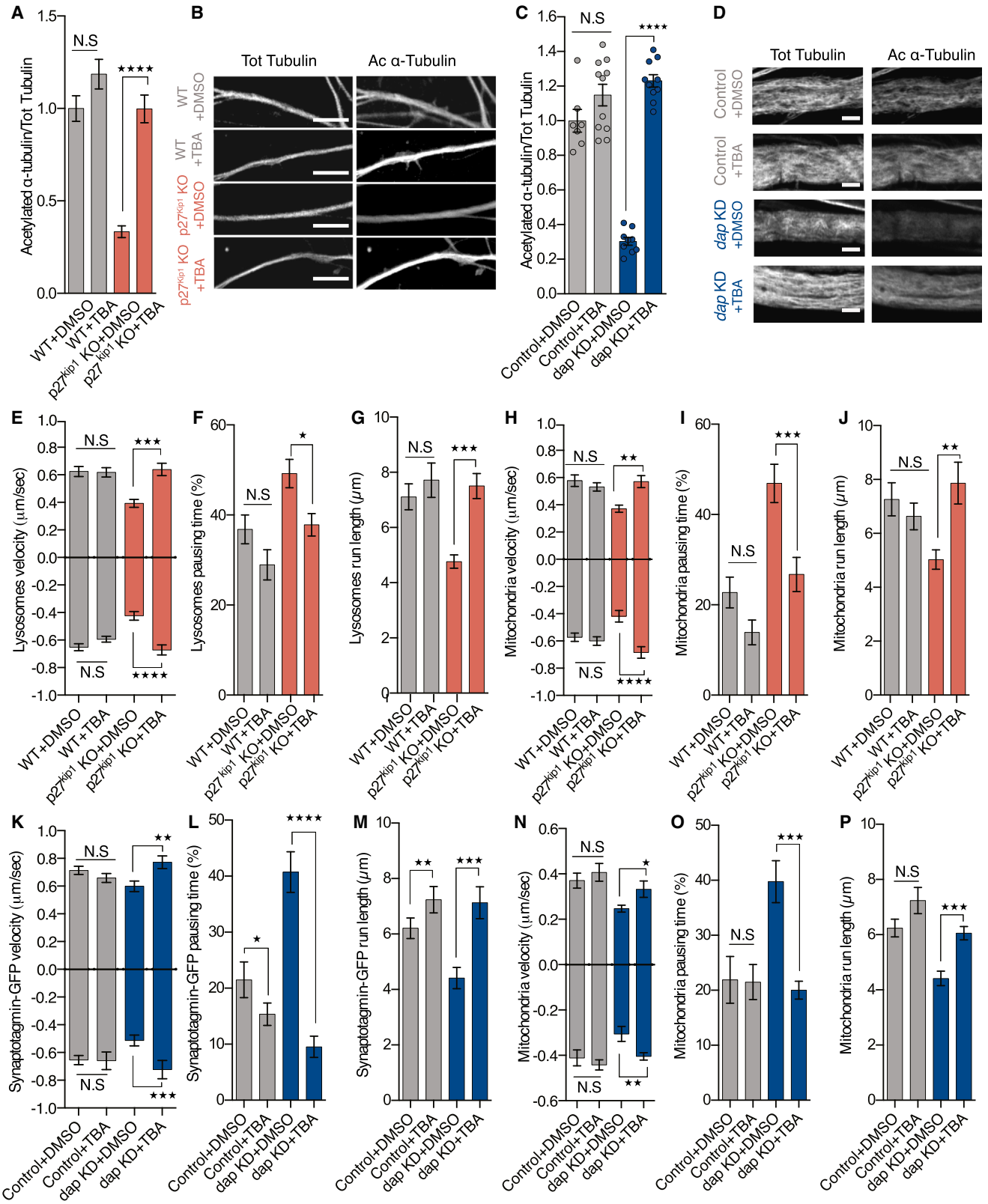

(legend on next page)

levels, as compared to Controls (Figures 4F–4I). These results support possible regulation of the ATAT1 protein level by $p27^{Kip1}$.

To test whether a reduction of ATAT1 protein expression underlies the axonal transport defects observed upon loss of $p27^{Kip1}$, we re-expressed ATAT1 in mice cortical projection neurons by *in utero* electroporation of ATAT1-GFP or GFP in E14.5 $p27^{Kip1}$ KO or WT embryos (Figures 4J–4O and S7C–S7H). The following day, the electroporated neuron progenitors were isolated and cultured for 7 DIV in microfluidic devices to track the axonal transport of lysosomes and mitochondria. Expression of ATAT1-GFP but not GFP rescued axonal transport defects (instantaneous and average transport velocities, pausing time, and run length) in $p27^{Kip1}$ KO cortical projection neurons (Figures 4J–4O and S7C–S7H), as well as MT-acetylation level (Figures S7I and S7J), without affecting the directionality of moving vesicles or mitochondria (Figures S7C, S7D, S7G, and S7H).

The protein $p27^{Kip1}$ is intrinsically unstructured and interacts with various non-cell-cycle proteins (Godin and Nguyen, 2014), an activity through which it can regulate protein stability in cortical progenitors (Nguyen et al., 2006a). Therefore, we tested whether $p27^{Kip1}$ stabilizes ATAT1 by protein interaction. Toward this purpose, we co-transfected $p27^{Kip1}$:RFP and ATAT1-GFP constructs in E14.5 cortical neurons, which co-localized in the soma and in the axon (Tau-1^{+}), where intense molecular transport occurs (Figure 5A). Next, we transfected HEK293 cells with ATAT1-GFP and $p27^{Kip1}$ or its variants that cannot promote cell-cycle exit ($p27^{Kip1}$ CK-) or MT polymerization ($p27^{Kip1}$ 4A) and performed co-immunoprecipitation assays and WB analyses on cell lysates. We showed that $p27^{Kip1}$ and its variants interact with ATAT1-GFP (Figures 5B and 5C). To understand better the nature of this interaction, we expressed either the N-terminal domain of p27 ($p27^{Kip1}$ N-Term, 1–88 amino acids [aa]) or its C-terminal portion ($p27^{Kip1}$ C-Term, 89–198 aa) and showed that only $p27^{Kip1}$ C-Term co-immunoprecipitates with ATAT1 (Figure 5D).

Next, we analyzed lysates from transfected HEK293 cells to test whether $p27^{Kip1}$ modulates the stability of ATAT1 upon addition of cycloheximide (50 μg/mL) (Meloni et al., 2005). We found that the expression of $p27^{Kip1}$ significantly extended the half-life time of ATAT1 as compared to Controls (Figures 6A and 6B), which was further supported by fluorescence microscopy analysis (Figures 6C and 6D). Moreover, $p27^{Kip1}$ 4A, $p27^{Kip1}$ CK-, and $p27^{Kip1}$ C-terminal increase ATAT1 stability to a similar extent, as compared to Control (Figures 6C–6H). However, as expected from co-immunoprecipitation assays (Figure 5D), the overexpression of $p27^{Kip1}$ N-terminal did not modulate the half-life of ATAT1 (Figures 6G and 6H). To test whether ATAT1 protein degradation was mediated by the proteasome, we co-treated HEK293 cells with MG132 (a potent inhibitor of the proteasome 26S subunit, 10 μM) together with cycloheximide. We found that MG132 treatment was as efficient as the overexpression of $p27^{Kip1}$ to increase ATAT1 stability (Figures 6I and 6J). Moreover, treatment of cultured mice $p27^{Kip1}$ KO cortical projection neurons with MG132 for 4 hr (Suh et al., 2005) increased the acetylation of α-tubulin to a level that is comparable to Control treatment (Figures 6K and 6L). These data suggest that $p27^{Kip1}$ stabilizes ATAT1 by preventing its proteasome-mediated degradation, thereby modulating MT acetylation and axonal transport (Figure 7).

DISCUSSION

The multifunctional $p27^{Kip1}$ protein is expressed at the onset of neurogenesis in cerebral cortical progenitors, as well as in newly generated post-mitotic neurons, where it coordinates different biological activities such as proliferation, migration, and differentiation (Godin et al., 2012; Kawauchi et al., 2006; Nguyen et al., 2006a). At the molecular level, the cytoplasmic pool of $p27^{Kip1}$ predominantly regulates cytoskeleton dynamics (Godin and Nguyen, 2014; Nguyen et al., 2006b). Among its cytoskeletal targets, $p27^{Kip1}$ binds to stathmin (Baldassarre et al., 2005) or directly to the MTs to control their polymerization and regulate cell migration (Godin et al., 2012). These molecular activities prompted us to investigate with a combination of *in vitro* and

Figure 3. HDAC6 Inhibition Rescues Axonal Transport Together with Tubulin Acetylation upon Loss of $p27^{Kip1}$ or Dacapo

(A and B) Immunolabeling quantification (A) and representative images (B) of acetylated α-tubulin (Ac α-tubulin) and tubulin (Tot Tubulin) in axons of cultured cortical neurons from E14.5 WT or $p27^{Kip1}$ KO embryos treated with 10 μM DMSO or TBA for 8 hr. Scale bar, 10 μm.

(A) Kruskal-Wallis ANOVA followed by Dunn post hoc tests. N for axons >30; N for animals 3 (WT with DMSO), 3 (WT with TBA), 3 ($p27^{Kip1}$ KO with DMSO), and 3 ($p27^{Kip1}$ KO with TBA) ($p < 0.0001$).

(C and D) Immunolabeling quantification (C) and representative images (D) of Ac α-tubulin and Tot Tubulin in motoneurons of Control and dap KD third instar larvae fed for 30 min before fixation with 10% sucrose solution supplemented with 1 mM DMSO. Scale bar, 10 μm.

(C) One-way ANOVA followed by the Bonferroni post hoc test; N for animals = 10 (Control with DMSO), 8 (Control with TBA), 6 (dap KD with DMSO), and 7 (dap KD with TBA) ($p < 0.0001$; $F = 71.85$).

(E–J) Histograms of live imaging of axons from projection neurons cultured in microfluidic devices showing transport velocity (E and H), pausing time (F and I), and run length (G and J) of lysosomes and mitochondria treated with 10 μM DMSO or TBA for 8 hr. Kruskal-Wallis ANOVA followed by Dunn post hoc tests. N for lysosomes or mitochondria >250; N for animals = 4 (WT) and 5 ($p27^{Kip1}$ KO) treated with DMSO or TBA. For instantaneous velocity of cargoes (E and H), $p = 0.0002$ for anterograde and $p < 0.0001$ for retrograde lysosomes; $p = 0.004$ for anterograde and $p < 0.0001$ for retrograde mitochondria. For pausing time (F and I), $p = 0.0002$ for lysosomes; $p < 0.0001$ for retrograde mitochondria. For run length (G and J), $p = 0.0006$ for lysosomes; $p = 0.0125$ for mitochondria.

(K–P) Histograms of live imaging of third instar larvae motoneurons *in vivo* to analyze transport velocity (K and N), pausing time (L and O), and run length (M and P) of synaptotagmin-GFP and Mito-GFP of larvae fed for 30 min with 10% sucrose solution supplemented with 10 μM DMSO or TBA. See also Figures S5 and S6.

(K–P) Kruskal-Wallis ANOVA followed by Dunn post hoc tests. N for vesicles >150; N for animals = 10 (Control with DMSO), 7 (Control with TBA), 8 (dap KD with DMSO), and 8 (dap KD with TBA); N for mitochondria >100; N for animals = 5 (Control with DMSO), 5 (Control with TBA), 6 (dap KD with DMSO), and 6 (dap KD with TBA). For instantaneous velocity of cargoes (K), $p = 0.0021$ for anterograde and $p = 0.0004$ for retrograde vesicles; (N) $p = 0.0006$ for anterograde and $p = 0.0025$ for retrograde mitochondria. For pausing time (L), $p < 0.0001$ for vesicles. (O), $p = 0.0004$ for mitochondria. For run length (M), $p < 0.0001$ for vesicles; (P), $p < 0.0001$ for mitochondria.

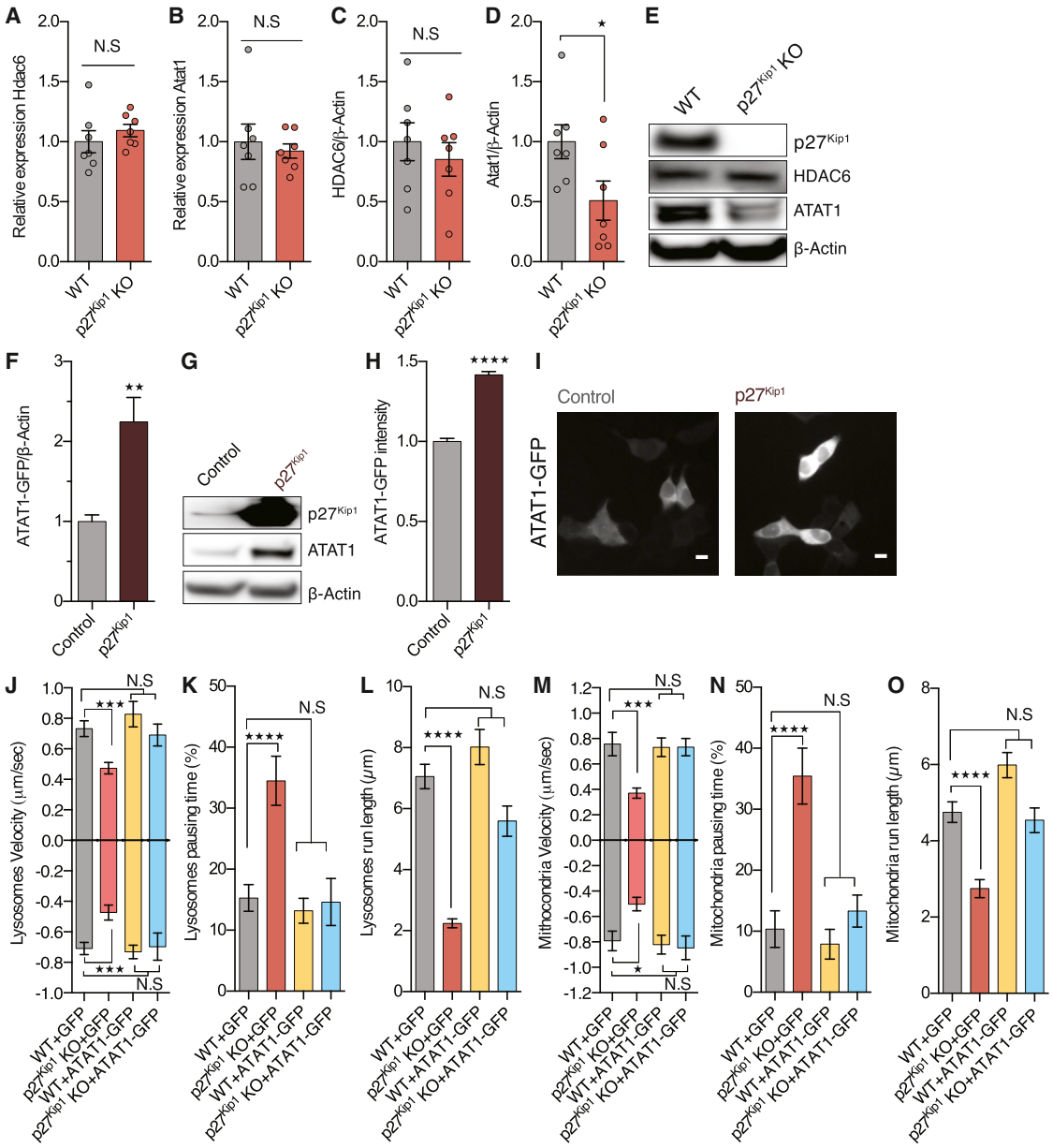

Figure 4. p27^{Kip1} Modulates Axonal Transport by Regulating ATAT1 Protein Expression

(A and B) qPCR analyses of Atat1 (A) and Hdac6 (B) mRNA levels from P0 WT or p27^{Kip1} KO mice.

(C–E) Quantification (C and D) and WB (E) of HDAC6 (C and E) and ATAT1 (D and E) protein levels in P0 WT or p27^{Kip1} KO mice.

(A–D) Unpaired two-tailed Student's t test. N for animals = 7 (WT) and 7 (p27^{Kip1} KO). (For qPCR: Atat1 p = 0.6338, HDAC6 p = 0.3974; for WB: ATAT1 p = 0.0411, HDAC6 p = 0.2022).

(F and G) Quantification (F) and WB(G) of ATAT1 levels in HEK293 transfected with ATAT1-GFP and RFP (Control) or p27^{Kip1}:RFP (p27^{Kip1}) constructs.

(H and I) ATAT1-GFP relative fluorescence quantification (H) and representative images (I) in HEK293 co-transfected with ATAT1-GFP and RFP (Control) or p27^{Kip1}:RFP (p27^{Kip1}) constructs. Scale bars, 10 μm.

(F and H) Unpaired two-tailed Student's t test, N = 7 for Control or p27^{Kip1}.

(J–O) Live imaging of axons from p27^{Kip1} KO E14.5 mice embryos, *in utero* electroporated with either ATAT1-GFP or Control (GFP) plasmids, and cultured at E15.5 for 7 DIV in microfluidics devices to analyze transport parameter, including instantaneous velocities (J and M), pausing time (K and N), and run length (L and O) of lysosomes (LysoTracker) or mitochondria (MitoTracker). See also Figure S7.

(J–O) Kruskal-Wallis ANOVA followed by Dunn post hoc comparison test. N for lysosomes or mitochondria >150; N for animals = 3 (WT+GFP), 3 (WT+ATAT1-GFP), 3 (p27^{Kip1} KO+GFP), and 3 (p27^{Kip1} KO+ATAT1-GFP). For instantaneous velocity of cargoes (J and M), p = 0.0004 for anterograde and p = 0.0005 for retrograde lysosomes; p = 0.0002 for anterograde and p = 0.014 for retrograde mitochondria. For pausing time (K and N), p < 0.0001 for lysosomes and p < 0.0001 for mitochondria. For run length (L and O), p < 0.0001 for lysosomes and mitochondria.

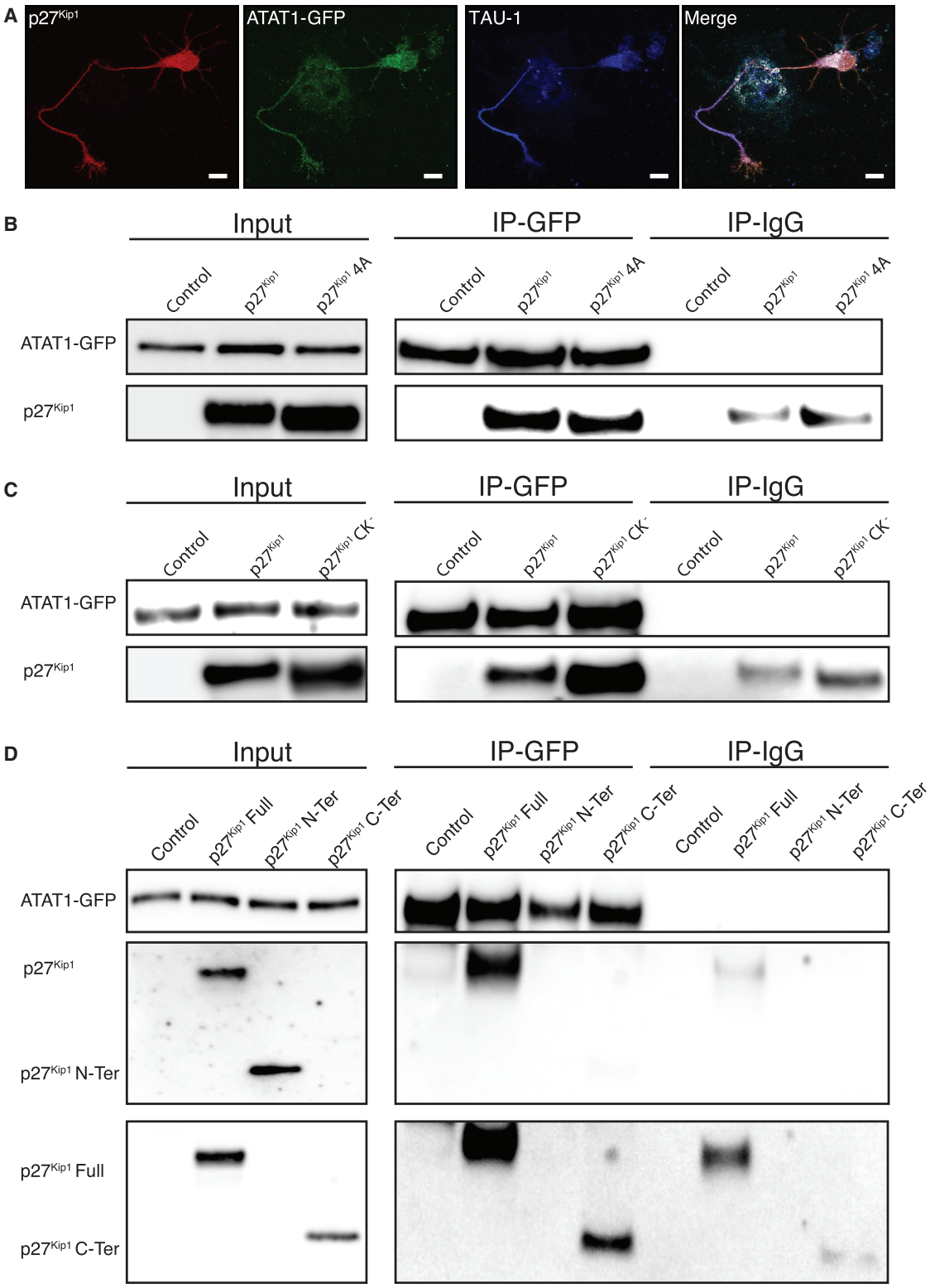

(legend on next page)

in vivo analyses the possible contribution of p27^{Kip1} to MT-dependent axonal transport.

A great variety of molecular motors transport organelles and vesicles along MTs in axons by selectively binding to adaptor proteins (Hirokawa et al., 2010). However, p27^{Kip1} and Dacapo are unlikely to modulate axonal transport via specific motors or adaptors since we observed a global impact on anterograde and retrograde transport upon their depletion. Indeed, both proteins interact with MTs, and as such we hypothesized that they modulate molecular transport via regulation of the axonal MTs. Our data validated this hypothesis, although we were surprised to find that the function of p27^{Kip1} in axonal transport does not require its MT-polymerization domain (Godin et al., 2012), but rather the integrity of its C-terminal portion to stabilize ATAT1, which promotes MTs acetylation. This activity of p27^{Kip1} C-Term is comparable to the ability of the p27^{Kip1} N-Term to promote the stabilization of other proteins such as Ngn2 in cortical progenitors (Nguyen et al., 2006a), suggesting an important scaffolding activity for p27^{Kip1} with multiple protein partners in distinct cytoplasmic compartments of different cells within the developing cortex.

More specifically, we showed that the loss of *p27^{Kip1}* resulted in the reduction of ATAT1 protein levels, thereby leading to the reduction of α-tubulin acetylation followed by axonal transport defects. It is noteworthy that increasing the acetylation of MTs improves axonal transport defects that result from inheritable mutations associated with Huntington and Parkinson diseases (Dompierre et al., 2007; Godena et al., 2014). Accordingly, we experimentally raised the acetylation of α-tubulin in neurons depleted for *p27^{Kip1}* or *dacapo* by blocking the activity of the tubulin deacetylase HDAC6. This treatment not only rescued axonal transport defects but it also improved the locomotor activity of *dap* KD larvae and flies. Impaired axonal transport is a common hallmark of many neurodevelopmental and neurodegenerative disorders (Gauthier et al., 2004; Godena et al., 2014; Lefler et al., 2015; Millecamps and Julien, 2013), and reduced levels of p27^{Kip1} have been detected in motoneurons from animal models of sporadic amyotrophic lateral sclerosis (ALS) (Jensen et al., 2016; Chakkalakal et al., 2014). Along this line, our data support a role for Dacapo in motoneuron axonal transport, the depletion of which leads to a reduction in locomotor activity similar to the one observed in ALS fly models (Romano et al., 2015).

Here, we show that either the deletion of p27^{Kip1} in cortical projection neurons or its fly ortholog Dacapo in larva motoneurons disrupts the transport of vesicles and mitochondria by interfering with the acetylation of α-tubulin in MTs, which is mediated by ATAT1. Specifically, our data suggest that the C-terminal domain p27^{Kip1} stabilizes ATAT1, possibly by preventing its proteasome-mediated degradation. Therefore, our work proposes a combinatorial role for these proteins in axonal transport that is conserved across species. By describing this non-canonical role for p27^{Kip1} and Dacapo in the nervous system, we further support the coordinator status of these proteins to couple multiple pathways that are important for the differentiation and functional maturation of neurons. The combinatorial roles played by p27^{Kip1} in different cellular compartments likely require the existence of different pools of p27^{Kip1}, whose specific dynamic regulation remains to be elucidated fully.

EXPERIMENTAL PROCEDURES

Mice

NMRI, *p27^{Kip1}* KO, CK-, and lox/lox mouse lines were housed under standard conditions and treated according to the guidelines of the Belgian Ministry of Agriculture in agreement with the European Community Laboratory Animal Care and Use Regulations (86/609/EEC, Official Journal of the European Communities L358, December 18, 1986). Female and male mice were harvested either at E14.5 or E15.5 for axonal transport assays or at P0 for biochemical assays.

Drosophila Lines Maintenance and Crosses

Flies were kept in a 25°C incubator under 12-hr light and dark cycles. All of the crosses were performed at 25°C; hatched first instar larvae were transferred in a 29°C incubator until use. For axonal transport, behavioral experiments and immunostaining D42-Gal4-UAS:Syt-GFP, D42-Gal4-UAS:Mito-GFP, D42-Gal4-UAS:LAMP1-GFP (Soukup et al., 2016) or D42-Gal4 virgin females were crossed with UAS-RNAi fly lines. For qPCR analysis, actin-Gal4 (Bloomington 4414) females were crossed with UAS-RNAi fly lines. UAS:*zpg* RNAi (CG10125) were used as Controls (Vienna *Drosophila* Resource Center); UAS:*dacapo* RNAi were received from N. Perrimon and P(w^{+},*dap*1gm)III.1 (Meyer et al., 2002).

Reagents and Antibodies

TBA, MG132, and cycloheximide were obtained from Sigma-Aldrich (SML0044, M7449, and C104450, respectively). Antibodies were used for WB to detect tubulin (DM1A, Sigma-Aldrich, catalog no. T9026, 1:5,000), acetylated tubulin (6-B11-1, Sigma-Aldrich, catalog no. T7451, 1:15,000), β-actin (Sigma-Aldrich, catalog no. A3853, 1:20,000), HDAC6 (Santa Cruz Biotechnology, catalog no. sc-5258, 1:200), p27^{Kip1} (Santa Cruz Biotechnology, catalog no. sc-528, 1:500), p27^{Kip1} (Santa Cruz Biotechnology, catalog no. sc-1641, 1:500), GFP (Molecular Probes, catalog no. A11122, 1:1,000), and ATAT1 (gift from M. Nachury, 1:1,000). The following Jackson ImmunoResearch Laboratories peroxidase conjugated antibodies were used at 1:10,000 (80 ng/mL): goat anti-mouse (catalog no. 115-035-003), goat anti-rabbit (catalog no. 111-035-003), and donkey anti-goat (catalog no. 705-035-003). For mouse immunostaining, we used antibodies against GFP (Nacalai Tesque, catalog no. 04404-26, 1:500), Tau-1 (Millipore, catalog no. MAB3420, 1:500), acetylated tubulin (Sigma-Aldrich, catalog no. T6793, 1:15,000), tubulin (Cytoskeleton, catalog no. ATN02-A, 1:150), β-3 tubulin (Covance, catalog no. MMS-435P-0100, 1:1,000), and p27^{Kip1} (Santa Cruz Biotechnology, catalog no. sc-528, 1:200).

For immunostaining third instar larvae, we used antibodies against CSP (*Developmental Studies Hybridoma Bank*, DCSP-2 [D6D], 1:10) from S. Benzer, NP1 (*Developmental Studies Hybridoma Bank* 1:50) from I. Hariharan, horseradish peroxidase (HRP) (Sigma-Aldrich, catalog no. P97899, 1:1,000), acetylated tubulin (Sigma-Aldrich, catalog no. T6793, 1:15,000), and tubulin (Cytoskeleton, catalog no. ATN02-A, 1:150).

Figure 5. p27^{Kip1} Binds and Colocalizes with ATAT1

(A) Immunolabeling of an E14.5 mouse cortical neuron Tau-1^{+} (blue) transfected with p27^{Kip1}:RFP (red) and ATAT1-GFP (green) and cultured 7 DIV. Scale bar, 10 μm.

(B–D) Co-immunoprecipitation analysis of p27^{Kip1} variants with ATAT1-GFP using GFP antibody or general IgG antibody as Control by WB on extracts from HEK293 cells co-transfected with (B) Control (RFP), p27^{Kip1} (p27^{Kip1}:RFP) or p27^{Kip1} 4A (p27^{Kip1} 4A:RFP); (C) Control (pCDNA3.1 empty vector), p27^{Kip1}, or p27^{Kip1} CK-; (D) Control (pCS2^{+} empty vector), p27^{Kip1}, p27^{Kip1} N-Terminal (1–88 aa), and p27^{Kip1} C-Terminal (89–198 aa).

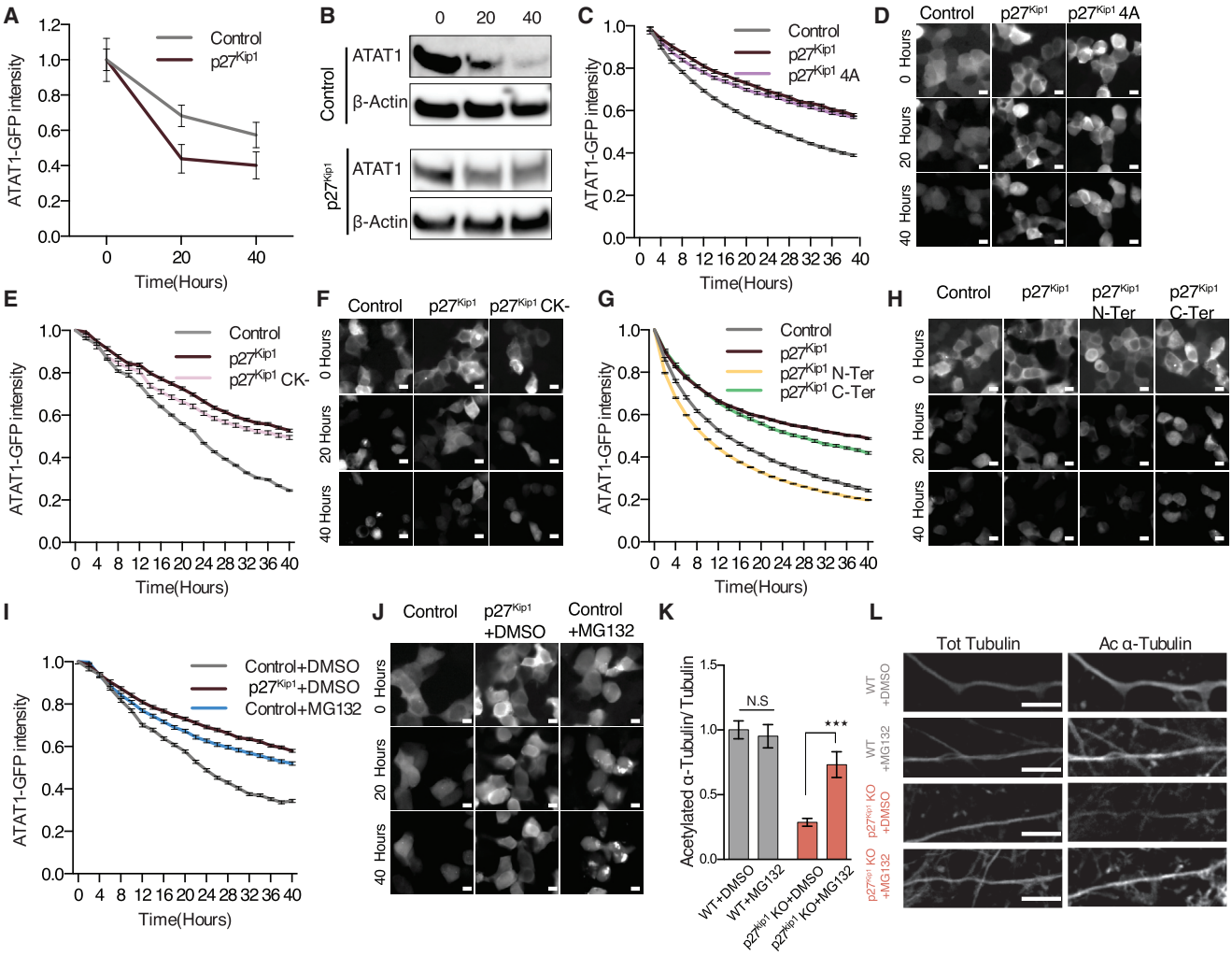

Figure 6. p27^{Kip1} Regulates ATAT1 Stability

(A–J) Protein degradation assays from HEK293 cells co-transfected with ATAT1-GFP and p27^{Kip1} variants, as indicated in the figures. Cells were incubated 24 hr post-transfection with 50 μg/mL cycloheximide (CHX) for 40 hr and where indicated, 10 μM DMSO or MG132 (I and J). ATAT1-GFP levels were measured by WB (A and B) at time points 0, 20 min (20), and 40 min (40) or by fluorescence microscopy (C–J) every 2 hr. WB and its quantification of ATAT1-GFP co-transfected with Control (RFP) or p27^{Kip1} (p27^{Kip1}:RFP) and immunoblotted with ATAT1 and β-actin antibodies (A and B). Fluorescent intensity quantification and representative images of HEK293 cells co-transfected with ATAT1-GFP (ATAT1-GFP) and Control (RFP), p27^{Kip1} (p27^{Kip1}:RFP), or p27^{Kip1} 4A (p27^{Kip1} 4A:RFP) (C and D). Control (pCDNA3.1 empty vector), p27^{Kip1}, or p27^{Kip1} CK- (E and F). Control (pCS2^{+} empty vector), p27^{Kip1}, p27^{Kip1} N-Terminal (1–88 aa), and p27^{Kip1} C-Terminal (89–198 aa) (G and H). Control (RFP) + 10 μM DMSO, Control (RFP) + 10 μM MG132, or p27^{Kip1} (p27^{Kip1}:RFP) + 10 μM DMSO (I and J). Scale bar, 10 μm.

(A) Two-way ANOVA, p = 0.046 for variation between groups, N = 12.

(C, E, G, and I) Two-way ANOVA; p < 0.0001 for variation among groups; N >6,000 cells per well; nine fields were analyzed per well from six wells per group.

(K and L) Immunolabeling quantification (K) and representative images (L) of Ac α-tubulin (gray) and Tot Tubulin (red) in axons of cultured cortical neurons from E14.5 WT or p27^{Kip1} KO embryos treated with 10 μM DMSO or MG132 for 4 hr. Scale bar, 10 μm.

(K and L) Kruskal-Wallis ANOVA followed by Dunn post hoc tests. N for axons >30; N for animals 3 (WT with DMSO), 3 (WT with MG132), 3 (p27^{Kip1} KO with DMSO), and 3 (p27^{Kip1} KO with MG132) (p = 0.0002).

Immunofluorescence

E14.5 mice brain sections were fixed 30 min in 4% paraformaldehyde (PFA), sectioned and stained for the detection of p27^{Kip1} using blocking (0.3% PBS, 10% Triton-X, and normal donkey serum) for 1 hr at room temperature (RT), and incubation overnight with primary antibodies at 4°C and with secondary antibodies for 1 hr at RT. Cultured cortical neurons were fixed with ice-cold methanol for 5 min at −20°C for immunolabeling using blocking (0.3% PBS, 10% Triton-X, and normal donkey serum) for 1 hr at RT and incubation overnight with primary antibodies at 4°C and with secondary antibodies for 1 hr at RT. Antigen retrieval (10 mM sodium citrate, pH 8.5, at 60°C) was performed for 1 hr for p27^{Kip1}, GFP, and Tau-1 immunolabeling. Third instar larvae were dissected and fixed with 4% PFA for 20 min at RT. Larvae were blocked (0.2% PBS [CSP staining] or 0.3% Triton-X [tubulin acetylation staining] and 1% BSA [Sigma-Aldrich, catalog no. A2058]) for 30 min at RT, and incubated

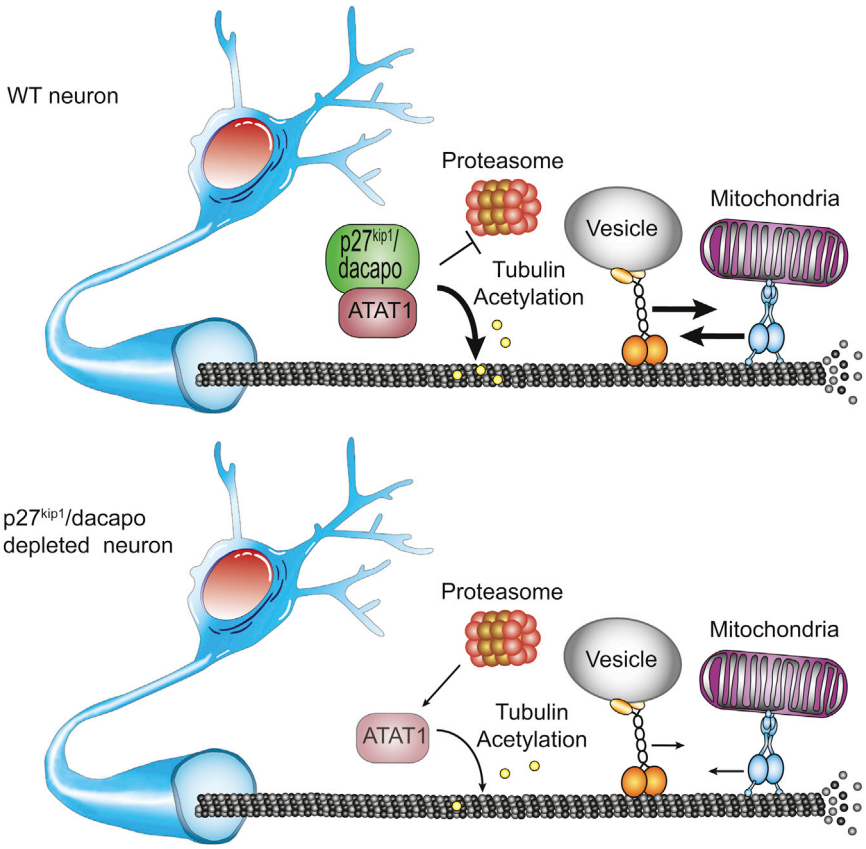

Figure 7. Working Model

Scheme depicting the molecular activity of $p27^{Kip1}$/dacapo in axonal transport via its interaction with the MT acetyltransferase ATAT1. When $p27^{Kip1}$ is not expressed, ATAT1 is less stable, likely because it is more easily processed by the proteasome. This leads to an overall reduction of the acetylation of MTs and impaired axonal transport.

with primary antibodies at 4°C and with secondary antibodies at RT for 2 hr. For NP1, staining larvae were fixed in 16% formaldehyde:Buffer B (100 mM KH_2PO_4, pH 6.8, 450 mM KCl, 150 mM NaCl, and 20 mM $MgCl_2$):H_2O at a ratio of 2:1:3 and stained according to published work (Hong et al., 2003). All of the images were acquired with a Nikon A1 Ti. Immunolabelings of RFP, GFP and Tau-1 were acquired with the Airyscan super-resolution module on a Zeiss LSM-880 confocal microscope.

Image Analyses

Fluorescence intensity levels were measured with ImageJ (https://imagej.net/Fiji/Downloads), using 30-μm-long regions of interest (ROIs), accounting for the full width of the axons. Mean intensity levels after background subtraction were used to calculate the ratio of acetylated tubulin/tubulin, ATAT1-GFP/pCAGGS:RFP, or Dacapo/HRP.

Microfluidics Devices Fabrication and Axonal Transport Recording *In Vitro* and *In Vivo*

Microfluidics devices were prepared as published (Gluska et al., 2016). Briefly, E14.5 cortices were mechanically dissociated in Hank's balanced salt solution (HBSS) supplemented with 1.5% glucose and brain-derived neurotrophic factor (BDNF) (PeproTech, catalog no. 450-02) 50 ng/mL in the distal side and 20 ng/mL in the soma side. Cells were cultured at a confluence of ~70% with Neurobasal Medium (Thermo Fisher, catalog no. 21103049) supplemented with 2% B27 (Thermo Fisher, catalog no. 17504044), 1% penicillin/streptomycin (Thermo Fisher, catalog no. 15140122), and 0.125% GlutaMAX (Thermo Fisher, catalog no. 35050061). Recordings were made after 7 DIV by adding 1 μM LysoTracker Red DND-99 (Thermo Fisher, catalog no. L7528), MitoTracker Green FM (Thermo Fisher, catalog no. M7514), or MitoTracker Deep Red FM (Thermo Fisher, catalog no. M22426) 30 min before time-lapse recordings. Cultured neurons were incubated with 10 μM TBA for 8 hr before recording. The microscope chamber was heated to 37°C and supplied with 5% CO_2 for live recording. For recording in *Drosophila* motoneurons, third instar larvae were anesthetized in ether vapors for 8 min and mounted dorsally on the microscope slide and gently pressed with a coverslip (Zala et al., 2013). Drug treatment of third instar larvae was performed by incubating larvae in 10% sucrose solution supplemented with 1 M TBA or DMSO for 30 min before recording. Live imaging was performed using an inverted confocal microscope (Nikon A1 Ti) at 600-ms frame intervals. Kymographs were generated for single-blind analysis using ImageJ plugin-KymoToolBox (fabrice.cordelieres@curie.u-psud.fr). Vesicles were considered stationary at <0.1 μm/s. For the *Drosophila* analysis, the ImageJ StackReg plugin was used to align frames.

qPCR Analysis

For qRT-PCR, mice brain cortices were collected in TRIzol (Ambion, Life Technologies) followed by RNA extraction according to the manufacturer's instructions. After DNase treatment (Roche), 1 μg RNA was reverse transcribed with RevertAid Reverse Transcriptase (Fermentas). Real-time PCR was performed on a Light Cycler 480 (Roche) using SYBR Green mix according to the manufacturer's instructions. The following primers were used:

dacapo: fw GTCAGCTTCCAGGAGTCGAG; rev CCAAAGTTCTCCCGTTCTGA; *Atat1*: fw TGTAGATGAGCTGGGCAAGG; rev ATAACGTGCCGGTTGCTTTG; *Hdac6*: fw. GGAGACAACCCAGTACATGAATGAA; rev CGGAGGACAGAGCCTGTAG; *actin:* fw GACGGCCAGGTCATCACTAT; rev ATGCCACAGGATTCCATACC; *36b4*: fw ATGGGTACAAGCGCGTCCTG; rev GCCTTGACCTTTTCAGTAAG; *TBP*: fw CCACGGTGAATCTGTGCT; rev GGAGTCGTCCTCGCTCTT; *RpL13* fw AGCTGAACCTCTCGGGACAC; rev TGCCTCGGACTGCCTTGTAG.

Analyses were performed using the $2^{-\Delta\Delta}$CT method after defining primer efficiencies (Morelli et al., 2016).

Western Blot

Mouse brain cortices were homogenized on ice in radioimmunoprecipitation assay (RIPA) buffer with protease inhibitor cocktail (Sigma-Aldrich, PHOSSRO, catalog no. P8340 or catalog no. S8820) and 5 μM trichostatin-A (Sigma-Aldrich, catalog no. T8552). For α-tubulin acetylation, 2 μg protein lysate were loaded on a gel and 20 μg protein were used to assess the expression of all of the other proteins. Membranes were imaged using Amersham Imager 600 (General Electric, catalog no. 29083461), and band densitometry was measured using ImageJ.

Locomotor Activity and Climbing Assay

Locomotion assays for third instar larvae were performed as previously described (Shaver et al., 2000). To test the effect of TBA on locomotor behavior, larvae were fed with 10% sucrose solution supplemented with either

1 mM TBA or DMSO for 30 min. The optimal concentration of TBA was selected after the concentration-response assay. A climbing assay for adult flies was performed as previously described (Chambers et al., 2013). To test the effect of TBA on climbing, newborn flies were fed for 5 days with 10% sucrose solution containing 1 mM TBA or DMSO.

Immunoprecipitation

The Pierce Crosslink immunoprecipitation kit (catalog no. 26147) was used following the manufacturer's instructions. Four micrograms of GFP (Sigma-Aldrich, catalog no. 11814460001) or general mouse immunoglobulin G (IgG) (Millipore, catalog no. 12-371). For the detection by WB of $p27^{Kip1}$, the N terminus Santa Cruz F-8 clone was used; for the detection of $p27^{Kip1}$, the full-length or C terminus Santa Cruz C-19 clone was used; and for detection of ATAT1, GFP antibody was used (Sigma-Aldrich, catalog no. 11814460001).

Purification of Dacapo Recombinant Protein

Dacapo was cloned in pET-16b vector. His-tagged Dacapo was expressed in the *Escherichia coli* BL21 (DE3) strain. Proteins were purified on TALON Metal affinity resin (Clontech) and dialyzed with general tubulin buffer (80 mM PIPES, pH 6.9; 2 mM $MgCl_2$; 0.5 mM EGTA). The purified proteins were analyzed by SDS-PAGE gel.

In Vitro Microtubule-Binding Assays

MTs were polymerized *in vitro* and stabilized with taxol (20 μM) using the MTs/Tubulin Biochem Kit (Cytoskeleton). Purified His-tagged Dacapo proteins were incubated at 37°C for 30 min with polymerized MTs in BRB80 buffer (80 mM PIPES, pH 6.8; 1 mM $MgCl_2$; and 1 mM EGTA supplemented with 1 mM guanosine triphosphate [GTP]). The reaction was then centrifuged for 30 min at 37°C at 100,000 × *g* to separate MT-associated from MT-soluble proteins. MTs were resuspended in general tubulin buffer (v/v). The same volume of each fraction was loaded on SDS-PAGE gels and analyzed by WB (tubulin, Dacapo).

Tubulin Polymerization Assay

A total of 30 μg purified tubulin (Cytoskeleton) were polymerized with 1 μM His-Dacapo protein in 20 μL reassembly buffer (100 mM 3-[*N*-morpholino]propanesulfonic acid [MOPS], pH 6.8; 0.1 mM EGTA; 0.5 mM $MgCl_2$, 0.5 mM GTP) for 30 min at 37°C. After centrifugation at 100,000 × *g* for 30 min at 37°C, pellets were resuspended in 20 μL reassembly buffer. Pellets and supernatants were analyzed by WB.

Plasmids

The plasmids encoding full-length $p27^{Kip1}$ and $p27^{Kip1}$ 4A (pCAGGS-$p27^{Kip1}$:RFP, pCAGGS-$p27^{Kip1}$4A:RFP) (Godin et al., 2012), as well as expression of Cre recombinase (pNeuroD-Cre:GFP and its corresponding pNeuroD-GFP), were described previously (Nguyen et al., 2006a). $pCS2^{+}$ plasmid was used as backbone for cloning either truncated or full-length $p27^{Kip1}$ (gift from A. Besson). pCDNA3.1 empty vector, pCDNA3.1-$p27^{Kip1}$, and pCDNA3.1-$p27^{Kip1}$ CK- were kindly provided by A. Besson. ATAT1-GFP (pEF5B-ATAT1-GFP) was purchased from Addgene (catalog no. 27099), (pEF5B-GFP) was subcloned from (pEF5B-ATAT1-GFP).

In Utero Electroporation

Mice were anesthetized with isoflurane (Abbott Laboratories) in an oxygen carrier before the administration of temgesic (Schering-Plough). Endotoxin-free plasmids (0.5–2 μg/μL) were injected into lateral ventricles of E14.5 mouse forebrain using a Femtojet microinjector (Eppendorf) followed by electroporation (5 pulses of 24 mV at 50-ms intervals for 950 ms) using platinum electrodes (Sonidel, catalog no. CUY650P3) connected to an electroporator (ECM 830, BTX).

Cycloheximide Chase Assay

HEK293 cells were plated at densities of 10,000 for 96-well plates and 80,000 for 24-well plates. The following day, cells were transfected using calcium phosphate with 0.05 μg/96-well plates or 0.2 μg/24-well plates of ATAT1-GFP plasmid and 0.1 μg/96-well plates or 0.4 μg/24-well plates of $p27^{Kip1}$ variant plasmid. For stability experience with $p27^{Kip1}$ N-Term and $p27^{Kip1}$ C-Term, the amount of control, $p27^{Kip1}$ N-Term, and $p27^{Kip1}$ C-Term was doubled (0.2 μg/96-well plates) compared to $p27^{Kip1}$ full-length plasmid because they were less efficiently expressed. Twenty-four hours post-transfection, 50 μg/mL cycloheximide were added to the well for 40 hr of incubation. For WB, the ATAT1 antibody was used for the detection of ATAT1-GFP and β-actin as loading control. For fluorescence microscopy analysis of ATAT1-GFP images, nine images per well were acquired every 2 hr and for a total of 40 hr post-addition of cycloheximide and MG132 using an IN Cell 2200 microscope (GE). The remaining ATAT1-GFP signal was determined by measuring GFP signal intensity from individual cells after the subtraction of background intensity levels. Analyses were performed using IN Cell Investigator developer software with the following parameters: segmentation: sensitivity 75, kernel size 50; and post-processing: waterclamp shed, fill holes, sieve objects >100 μm.

Analysis and Statistics

Data are presented as histograms of means ± SEMs. All of the experiments were performed under single- blind conditions, and the statistical analyses were generated with GraphPad Prism version 6.0. One-way ANOVA was used to analyze axonal transport, locomotor behavior, and immunolabeling in mice and *Drosophila*. Two-way ANOVA was used to analyze lysosome and mitochondria percentage of moving vesicles and the ATAT1-GFP cycloheximide chase assay. For qPCR, WB, *in vitro* MTs-binding assay, and some immunolabeling, either an unpaired two-tailed Student's t test or a two-sided Mann-Whitney test were used (*$p < 0.05$, **$p < 0.01$, ***$p < 0.001$, ****$p < 0.0001$).

SUPPLEMENTAL INFORMATION

Supplemental Information includes seven figures and can be found with this article online at https://doi.org/10.1016/j.celrep.2018.04.083.

ACKNOWLEDGMENTS

We thank N. Krusy and C. D'Alessandro for technical assistance. We are grateful to M. Nachury, N. Perrimon, and P. Verstreken for sharing reagents. We thank S. Ormenese and S. Freeman for assistance at the GIGA imaging platform. We thank E. Pichinuk at the Blavatnik Center for Drug Discovery in Tel-Aviv University for facilities use and help. A.E. and M.W. are supported by the Israel Science Foundation (grant no. 8811688). L.N. is supported by the Fonds de la Recherche Scientifique-Fonds de la Recherche Scientifique (FRS-FNRS, PDR DevoCortex-T.007315), the Fonds Léon Fredericq, the Fondation Médicale Reine Elisabeth, the Fondation Simone et Pierre Clerdent, the Belgian Science Policy (IAP-VII network P7/20), the Actions de Recherche Concertee (ARC) (ARC11/16-01), and the European Research Area Network Neuron (ERA-NET) STEM-MCD.

AUTHOR CONTRIBUTIONS

G.M., A.E., and L.N. designed the study. G.M. and A.E. performed and interpreted most of the experiments. R.L.B. contributed to the work on *Drosophila*. I.G.-N. and E.P. performed *in utero* electroporation and contributed to axonal transport experiments and super-resolution imaging. M.S. performed the immunoprecipitation experiments. J.D.G. performed the tubulin and polymerization assays. L.N. contributed to data interpretation. G.M., A.E., and L.N. wrote the manuscript with input from all of the co-authors.

DECLARATION OF INTERESTS

The authors declare no competing interests.

Received: December 19, 2017
Revised: March 22, 2018
Accepted: April 18, 2018
Published: May 22, 2018

REFERENCES

Baird, F.J., and Bennett, C.L. (2013). Microtubule defects & Neurodegeneration. J. Genet. Syndr. Gene Ther. *4*, 203.

Baldassarre, G., Belletti, B., Nicoloso, M.S., Schiappacassi, M., Vecchione, A., Spessotto, P., Morrione, A., Canzonieri, V., and Colombatti, A. (2005). p27(Kip1)-stathmin interaction influences sarcoma cell migration and invasion. Cancer Cell *7*, 51–63.

Besson, A., Gurian-West, M., Schmidt, A., Hall, A., and Roberts, J.M. (2004). p27Kip1 modulates cell migration through the regulation of RhoA activation. Genes Dev. *18*, 862–876.

Butler, K.V., Kalin, J., Brochier, C., Vistoli, G., Langley, B., and Kozikowski, A.P. (2010). Rational design and simple chemistry yield a superior, neuroprotective HDAC6 inhibitor, tubastatin A. J. Am. Chem. Soc. *132*, 10842–10846.

Chakkalakal, J.V., Christensen, J., Xiang, W., Tierney, M.T., Boscolo, F.S., Sacco, A., and Brack, A.S. (2014). Early forming label-retaining muscle stem cells require p27kip1 for maintenance of the primitive state. Development *141*, 1649–1659.

Chambers, R.P., Call, G.B., Meyer, D., Smith, J., Techau, J.A., Pearman, K., and Buhlman, L.M. (2013). Nicotine increases lifespan and rescues olfactory and motor deficits in a Drosophila model of Parkinson's disease. Behav. Brain Res. *253*, 95–102.

de Nooij, J.C., Letendre, M.A., and Hariharan, I.K. (1996). A cyclin-dependent kinase inhibitor, Dacapo, is necessary for timely exit from the cell cycle during Drosophila embryogenesis. Cell *87*, 1237–1247.

Dompierre, J.P., Godin, J.D., Charrin, B.C., Cordelières, F.P., King, S.J., Humbert, S., and Saudou, F. (2007). Histone deacetylase 6 inhibition compensates for the transport deficit in Huntington's disease by increasing tubulin acetylation. J. Neurosci. *27*, 3571–3583.

Fero, M.L., Rivkin, M., Tasch, M., Porter, P., Carow, C.E., Firpo, E., Polyak, K., Tsai, L.H., Broudy, V., Perlmutter, R.M., et al. (1996). A syndrome of multiorgan hyperplasia with features of gigantism, tumorigenesis, and female sterility in p27(Kip1)-deficient mice. Cell *85*, 733–744.

Friedmann, D.R., Aguilar, A., Fan, J., Nachury, M.V., and Marmorstein, R. (2012). Structure of the α-tubulin acetyltransferase, αTAT1, and implications for tubulin-specific acetylation. Proc. Natl. Acad. Sci. USA *109*, 19655–19660.

Gallastegui, E., Biçer, A., Orlando, S., Besson, A., Pujol, M.J., and Bachs, O. (2017). $p27^{Kip1}$ represses the Pitx2-mediated expression of $p21^{Cip1}$ and regulates DNA replication during cell cycle progression. Oncogene *36*, 350–361.

Gauthier, L.R., Charrin, B.C., Borrell-Pagès, M., Dompierre, J.P., Rangone, H., Cordelières, F.P., De Mey, J., MacDonald, M.E., Lessmann, V., Humbert, S., and Saudou, F. (2004). Huntingtin controls neurotrophic support and survival of neurons by enhancing BDNF vesicular transport along microtubules. Cell *118*, 127–138.

Gluska, S., Chein, M., Rotem, N., Ionescu, A., and Perlson, E. (2016). Tracking Quantum-Dot labeled neurotropic factors transport along primary neuronal axons in compartmental microfluidic chambers. Methods Cell Biol. *131*, 365–387.

Godena, V.K., Brookes-Hocking, N., Moller, A., Shaw, G., Oswald, M., Sancho, R.M., Miller, C.C., Whitworth, A.J., and De Vos, K.J. (2014). Increasing microtubule acetylation rescues axonal transport and locomotor deficits caused by LRRK2 Roc-COR domain mutations. Nat. Commun. *5*, 5245.

Godin, J.D., and Nguyen, L. (2014). Novel functions of core cell cycle regulators in neuronal migration. Adv. Exp. Med. Biol. *800*, 59–74.

Godin, J.D., Thomas, N., Laguesse, S., Malinouskaya, L., Close, P., Malaise, O., Purnelle, A., Raineteau, O., Campbell, K., Fero, M., et al. (2012). p27(Kip1) is a microtubule-associated protein that promotes microtubule polymerization during neuron migration. Dev. Cell *23*, 729–744.

Hirokawa, N., Niwa, S., and Tanaka, Y. (2010). Molecular motors in neurons: transport mechanisms and roles in brain function, development, and disease. Neuron *68*, 610–638.

Hong, A., Lee-Kong, S., Iida, T., Sugimura, I., and Lilly, M.A. (2003). The p27cip/kip ortholog dacapo maintains the Drosophila oocyte in prophase of meiosis I. Development *130*, 1235–1242.

Horiuchi, D., Barkus, R.V., Pilling, A.D., Gassman, A., and Saxton, W.M. (2005). APLIP1, a kinesin binding JIP-1/JNK scaffold protein, influences the axonal transport of both vesicles and mitochondria in Drosophila. Curr. Biol. *15*, 2137–2141.

Hubbert, C., Guardiola, A., Shao, R., Kawaguchi, Y., Ito, A., Nixon, A., Yoshida, M., Wang, X.F., and Yao, T.P. (2002). HDAC6 is a microtubule-associated deacetylase. Nature *417*, 455–458.

Janke, C., and Bulinski, J.C. (2011). Post-translational regulation of the microtubule cytoskeleton: mechanisms and functions. Nat. Rev. Mol. Cell Biol. *12*, 773–786.

Jensen, L., Jørgensen, L.H., Bech, R.D., Frandsen, U., and Schrøder, H.D. (2016). Skeletal Muscle Remodelling as a Function of Disease Progression in Amyotrophic Lateral Sclerosis. BioMed Res. Int. *2016*, 5930621.

Kawauchi, T., Chihama, K., Nabeshima, Y., and Hoshino, M. (2006). Cdk5 phosphorylates and stabilizes p27kip1 contributing to actin organization and cortical neuronal migration. Nat. Cell Biol. *8*, 17–26.

Lefler, S., Cohen, M.A., Kantor, G., Cheishvili, D., Even, A., Birger, A., Turetsky, T., Gil, Y., Even-Ram, S., Aizenman, E., et al. (2015). Familial Dysautonomia (FD) Human Embryonic Stem Cell Derived PNS Neurons Reveal that Synaptic Vesicular and Neuronal Transport Genes Are Directly or Indirectly Affected by IKBKAP Downregulation. PLoS One *10*, e0138807.

Maday, S., Twelvetrees, A.E., Moughamian, A.J., and Holzbaur, E.L. (2014). Axonal transport: cargo-specific mechanisms of motility and regulation. Neuron *84*, 292–309.

Meloni, B.P., Van Dyk, D., Cole, R., and Knuckey, N.W. (2005). Proteome analysis of cortical neuronal cultures following cycloheximide, heat stress and MK801 preconditioning. Proteomics *5*, 4743–4753.

Meyer, C.A., Kramer, I., Dittrich, R., Marzodko, S., Emmerich, J., and Lehner, C.F. (2002). Drosophila p27Dacapo expression during embryogenesis is controlled by a complex regulatory region independent of cell cycle progression. Development *129*, 319–328.

Millecamps, S., and Julien, J.P. (2013). Axonal transport deficits and neurodegenerative diseases. Nat. Rev. Neurosci. *14*, 161–176.

Morelli, G., Avila, A., Ravanidis, S., Aourz, N., Neve, R.L., Smolders, I., Harvey, R.J., Rigo, J.M., Nguyen, L., and Brône, B. (2016). Cerebral Cortical Circuitry Formation Requires Functional Glycine Receptors. Cereb. Cortex. *27*, 1863–1877.

Nguyen, L., Besson, A., Heng, J.I., Schuurmans, C., Teboul, L., Parras, C., Philpott, A., Roberts, J.M., and Guillemot, F. (2006a). p27kip1 independently promotes neuronal differentiation and migration in the cerebral cortex. Genes Dev. *20*, 1511–1524.

Nguyen, L., Besson, A., Roberts, J.M., and Guillemot, F. (2006b). Coupling cell cycle exit, neuronal differentiation and migration in cortical neurogenesis. Cell Cycle *5*, 2314–2318.

Poirier, K., Lebrun, N., Broix, L., Tian, G., Saillour, Y., Boscheron, C., Parrini, E., Valence, S., Pierre, B.S., Oger, M., et al. (2013). Mutations in TUBG1, DYNC1H1, KIF5C and KIF2A cause malformations of cortical development and microcephaly. Nat. Genet. *45*, 639–647.

Reed, N.A., Cai, D., Blasius, T.L., Jih, G.T., Meyhofer, E., Gaertig, J., and Verhey, K.J. (2006). Microtubule acetylation promotes kinesin-1 binding and transport. Curr. Biol. *16*, 2166–2172.

Romano, G., Appocher, C., Scorzeto, M., Klima, R., Baralle, F.E., Megighian, A., and Feiguin, F. (2015). Glial TDP-43 regulates axon wrapping, GluRIIA clustering and fly motility by autonomous and non-autonomous mechanisms. Hum. Mol. Genet. *24*, 6134–6145.

Shaver, S.A., Riedl, C.A., Parkes, T.L., Sokolowski, M.B., and Hilliker, A.J. (2000). Isolation of larval behavioral mutants in Drosophila melanogaster. J. Neurogenet. *14*, 193–205.

Soukup, S.F., Kuenen, S., Vanhauwaert, R., Manetsberger, J., Hernández-Díaz, S., Swerts, J., Schoovaerts, N., Vilain, S., Gounko, N.V., Vints, K., et al. (2016). A LRRK2-Dependent EndophilinA Phosphoswitch Is Critical for Macroautophagy at Presynaptic Terminals. Neuron *92*, 829–844.

Suh, J., Lee, Y.A., and Gwag, B.J. (2005). Induction and attenuation of neuronal apoptosis by proteasome inhibitors in murine cortical cell cultures. J. Neurochem. *95*, 684–694.

Zala, D., Hinckelmann, M.V., Yu, H., Lyra da Cunha, M.M., Liot, G., Cordelières, F.P., Marco, S., and Saudou, F. (2013). Vesicular glycolysis provides on-board energy for fast axonal transport. Cell *152*, 479–491.